IMDY: HUMAN INVERSE DYNAMICS FROM IMITATED OBSERVATIONS

Xinpeng Liu[1], **Junxuan Liang**[1], **Zili Lin**[1], **Haowen Hou**[2], **Yong-Lu Li**[1]*, **Cewu Lu**[1]*
[1]Shanghai Jiao Tong University, [2]Soochow University
xinpengliu0907@gmail.com, {whitefork,linzili111666}@sjtu.edu.cn
haowenhou@outlook.com, {yonglu_li,lucewu}@sjtu.edu.cn

ABSTRACT

Inverse dynamics (ID), which aims at reproducing the driven torques from human kinematic observations, has been a critical tool for human motion analysis. However, it is hindered from wider application to general motion due to its limited scalability. Conventional optimization-based ID requires expensive laboratory setups, restricting its availability. To alleviate this problem, we propose to exploit the recently progressive human motion imitation algorithms to learn human inverse dynamics in a *data-driven* manner. The key insight is that the human ID knowledge is implicitly possessed by motion imitators, though not directly applicable. In light of this, we devise an efficient data collection pipeline with state-of-the-art motion imitation algorithms and physics simulators, resulting in a large-scale human inverse dynamics benchmark as **Imitated Dynamics** (**ImDy**). ImDy contains over **150 hours** of motion with joint torque and full-body ground reaction force data. With ImDy, we train a data-driven human inverse dynamics solver **ImDyS(olver)** in a fully supervised manner, which conducts ID and ground reaction force estimation simultaneously. Experiments on ImDy and real-world data demonstrate the impressive competency of ImDyS in human inverse dynamics and ground reaction force estimation. Moreover, the potential of ImDy(-S) as a fundamental motion analysis tool is exhibited with downstream applications. The project page is https://foruck.github.io/ImDy.

1 INTRODUCTION

The rapid progress in human motion capture based on computer vision has made an enormous amount of human motion data available to the research community (Mahmood et al., 2019; Mandery et al., 2016). The accumulation of human motion manages to push motion understanding forward in various tasks, including behavior understanding (Punnakkal et al., 2021; Shahroudy et al., 2016) and character animation (Guo et al., 2022; Tevet et al., 2023). However, given the vision-based nature, most current efforts focus only on visible kinematics information. The invisible factors, especially the dynamic factors, which could carry deeper insights into the underlying production mechanism of human motion, are typically overlooked, such as *driven torques* and *ground reaction forces*. This limits the current motion understanding algorithms from wider applications to domains where physical constraints must be seriously considered, such as robotics, healthcare, and sports training. To alleviate this, we focus on identifying the driven torques and ground reaction forces for human motion from pure kinematics MoCap data, known as human inverse dynamics (ID).

Human inverse dynamics, as a basic step toward physical motion modeling, has been extensively discussed by the biomechanics community for applications like gait analysis. A fundamental obstacle is that it could not be measured non-intrusively. Therefore, computationally expensive optimization-based methods are widely adopted and mature software is developed (Delp et al., 2007; Damsgaard et al., 2006; Werling et al., 2021). However, accurately measured ground reaction forces are required to ensure a determinate solution, which could be expensive and applicable only in restricted laboratory settings. Also, the optimization process could be sensitive to small disturbances in either motion capture noises or subject vari-

*Corresponding authors.

ances. These make it hard to scale up for wider applications to general motion. Given the success achieved by data-driven methods in computer vision and natural language processing, deep-learning-based methods are proposed (Zell & Rosenhahn, 2015; Zell et al., 2017; Lv et al., 2016), aiming at scalable human inverse dynamics with only kinematic observations as inputs. Unfortunately, *data acquisition* becomes a major bottleneck since laboratory setups are still required for ground-truth acquisition.

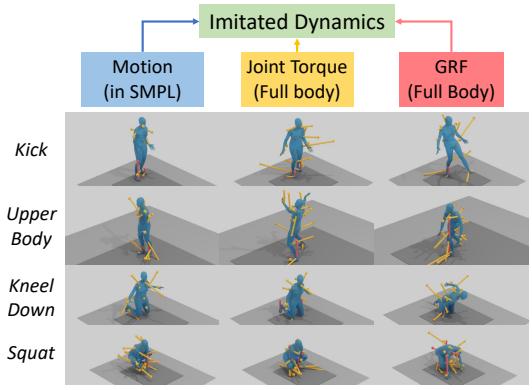

Figure 1: ImDy pairs diverse SMPL motion data with dynamics including full-body torques and ground reaction forces (GRF) like the right knee GRF for kneeling, which could be hard to achieve under conventional laboratory setups.

Given this, we project our sights on the recent progress of Imitation Learning (IL) (Luo et al., 2021; 2023), which replicates recorded human motion through fully simulated humanoids with physical control signals, namely, joint torques. A key insight is that with the goal of kinematics phenomenon imitation, IL might also *implicitly* imitate the dynamics production mechanism, known as ID. However, IL is not directly applicable to ID. Despite the visual resemblances between the recorded and simulated motion, kinematic errors still exist. These errors could be neglected for kinematic analyses, however, when it comes to dynamic analysis, they could be amplified drastically (Uchida & Seth, 2022). Moreover, existing successful IL algorithms are typically based on joint-actuated SMPL (Loper et al., 2015) avatars, whose physical properties and topology differ from real humans. To this end, extracting ID knowledge from IL becomes critical. Here, we adopt the state-of-the-art motion IL algorithm (Luo et al., 2023) and physics simulator (Makoviychuk et al., 2021) to imitate recorded motions, extracting the observed kinematic states, joint torques, and the ground reaction forces, resulting in a large-scale human inverse dynamics database named **Im**itated **Dy**namics (ImDy) with more than 150-hour human motion. There are two major merits of ImDy. First, it is *scalable*. Multiple samples could be concurrently collected in the simulator without expensive laboratory setups, which extends the border of ID data acquisition. As shown in Fig. 1, we could even pair some rather complex motions with ID data, which is hard to achieve in laboratories. Second, it is *holistic*. Beyond the ground reaction force and ID typically recorded in laboratories for previous efforts (Zell et al., 2020; Mourot et al., 2022; Han et al., 2023), the physics simulator enables us to access the GRFs and joint torques of all human body segments, as shown in Fig. 1.

With the accumulated data, we could address the human inverse dynamics in a fully supervised manner. Given the observed kinematics states that describe a motion transition in a certain period, we train a data-driven solver as ImDyS(olver) to estimate the ground reaction forces and the internal dynamics to drive the transition. We also devise losses to regulate ImDyS with forward dynamics awareness and motion plausibility constraints.

We demonstrate the efficacy of ImDyS through a wide span of experiments. First, we evaluate our method on ImDy for a basic performance illustration with simulated ImDy. Then ImDyS is evaluated on GroundLink (Han et al., 2023), which contains real-world ground reaction force. Furthermore, we demonstrate the efficacy of ImDy on the recent real-world human dynamics dataset AddBiomechanics (Werling et al., 2024).

Our contribution could be summarized as: (1) We propose a novel pipeline for human inverse dynamics data collection, introducing a large-scale benchmark as ImDy. (2) Based on ImDy, a data-driven ID solver is instantiated as ImDyS. (3) Extensive experiments are conducted with analyses of the proposed data-driven methodology, demonstrating the feasibility of ImDyS.

2 Background

Conventional Inverse Dynamics. Inverse dynamics, known as inferring forces/moments from kinematic observations, have been discussed for long in the biomechanics community. In this literature,

it is formulated as an optimization problem: given a representative model of a subject, the joint kinematics over time w.r.t. the subject model, and the external forces imposed on the subject, find the driving torques that produce the observed motion (Uchida & Delp, 2021). The Newtonian dynamic equations are involved as

$$M(q)\ddot{q} + C(q, \dot{q}) + G(q) = J\lambda + \tau, \tag{1}$$

where $M(q)$ is the generalized human inertia matrix w.r.t. generalized coordinate q, $C(q, \dot{q})$ is the Coriolis and centrifugal forces, $G(q)$ represents gravity, J is the Jacobian matrix mapping external forces λ to the generalized coordinates. Thus, the driven torques τ could be obtained by minimizing the difference between the left and right terms of Eq. 1. Mature software based on this has been developed like OpenSim (Delp et al., 2007), AnyBody (Damsgaard et al., 2006), and Nimble (Werling et al., 2021). In addition, many efforts are made for clinical motion analysis (Fukuchi et al., 2018; Schreiber & Moissenet, 2019). However, these efforts are not as extensively recognized by the computer vision and computer graphics community as expected due to the scalability issue. Despite the elegant formulation, the efficacy of optimization-based heavily relies on the quality of external force λ (like GRF) measurement, whose cost could be non-trivial. Therefore, most of them focused on limited motion in laboratory settings. Some resort to wearable devices (Latella et al., 2016; 2019) to partially mitigate the limitation. In addition, fitting the raw captured kinematic observations to a specific human model for joint kinematics could be time-consuming and unstable, even with recent progress on it (Keller et al., 2023; Werling et al., 2023).

Learning-based Inverse Dynamics. With the progress in deep learning, there have been efforts to adopt neural networks to address the human ID problem. Many efforts focus on lower-body-only (Johnson & Ballard, 2014; Xiong et al., 2019) or upper-body-only (Manukian et al., 2023) inverse dynamics. More recently, Lv et al. (2016) collected over 1 hour of motion with an optical MoCap system, four force plates, and a pair of pressure insoles. The ground truth was obtained through optimization and a Gaussian mixture framework was devised. Zell & Rosenhahn (2015); Zell et al. (2017); Zell & Rosenhahn (2017) introduced a predictive dynamics-based human modeling for the acquisition of ground truth. Hundreds of motions were collected and different data-driven techniques were adopted for joint torque regression. Zell et al. (2020) proposed a weakly supervised method based only on motion for gait analysis. These efforts were constrained by costly data acquisition in real-world scenarios, resulting in limited data scale. Very recently, Werling et al. (2024) aggregated multiple existing biomechanics datasets, considerably boosting the data scale. However, most of the collected sequences contained only regular exercise motion with limited diversity. Some efforts focused on ground reaction forces such as (Rempe et al., 2020; Scott et al., 2020), UnderPressure (Mourot et al., 2022), and GroundLink (Han et al., 2023). Some recent works incorporated inverse dynamics into vision-based markerless MoCap systems. Shimada et al. (2021) and Li et al. (2022) simultaneously captured motion and joint torques with customized fully differentiated pipelines. A series of works (Yi et al., 2022; Gartner et al., 2022; Gärtner et al., 2022; Huang et al., 2022; Wang et al., 2023) imitated the captured motion in physical simulators with PD controllers and obtained the torques. However, an inherent problem is the amplification effect from kinematic errors to dynamic errors. As measured by Uchida & Seth (2022), only a 2-cm uncertainty of marker placement in a marker-based MoCap system could result in a peak ankle plantarflexion moment of 26.6 $N \cdot m$. Considering the precision of current markerless MoCap algorithms, the accuracy of the accompanied inverse dynamics could be questionable. Also, among all these efforts for learning-based inverse dynamics, only a few (Zell et al., 2017; Zell & Rosenhahn, 2017; Zell et al., 2020) were quantitatively evaluated with limited locomotion data. A scalable benchmark for learning-based inverse dynamics is still not available.

Motion Imitation. IL for human motion replicates recorded human motion sequences with physically controlled simulated characters, which could be inherently close to ID. Most early efforts focus on specified usages with limited generalizability (Bergamin et al., 2019; Peng et al., 2021; Won et al., 2021; 2022; Peng et al., 2022). With residual force control (Yuan & Kitani, 2019), which imposed supernatural forces at the root joint of the humanoid, Luo et al. (2021) generalized to 97% sequences in AMASS (Mahmood et al., 2019). Luo et al. (2023) eliminated the supernatural root force and achieved a 98.9% success rate on AMASS with fall-state recovery. The progress in human motion IL makes it possible to collect human-like motions with full dynamics, shedding new light on the scalable human ID data collection.

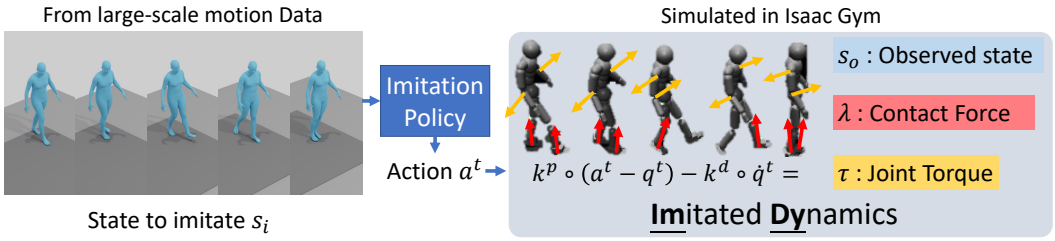

Figure 2: ImDy construction. We first train a motion imitation policy following Luo et al. (2023). Then, the policy is adopted to imitate arbitrary motions, with the imitated states recorded as ImDy.

3 Constructing Imitated Dynamics

ImDy aims to exploit the inherent closeness of inverse dynamics and imitation learning. Generally, the inverse dynamics (ID) and imitation algorithms (IL) could be abstracted as

$$\tau = ID(s_o^t, s_o^{t+1}),\ \tau = IL(s_o^t, s_i^{t+1}), \tag{2}$$

with driven torque τ, timestamp t, observed kinematic states s_o, and the state to imitate s_i. Both ID and IL learn the dynamic production mechanism of human motion. However, IL algorithms are not directly applicable to ID due to the non-equivalence between s_o^{t+1} and s_i^{t+1}. The errors in kinematics could be magnified in dynamics (Uchida & Seth, 2022). This also makes ID algorithms that are deeply coupled with markerless MoCap less reliable. However, it is possible to extract knowledge from IL for ID. In this section, we introduce a simple but effective ID data collection pipeline with IL algorithms. First, the adopted IL algorithm (Luo et al., 2023) is briefly covered in Sec. 3.1. Then, the data collection pipeline is introduced in Sec. 3.2. An overview is given in Fig. 2.

3.1 Imitation Learning Basics

A motion imitator $\pi(a^t|s_o^t, s_i^t)$ is trained following Luo et al. (2023) to solve the Markov Decision Process $\mathcal{M} = \langle \mathcal{T}, \mathcal{S}, \mathcal{A}, \mathcal{R}, \gamma \rangle$. The transition dynamics $\mathcal{T}$ and states $\mathcal{S}$ are governed by the physics simulator. For each timestamp t, the policy π produces action $a^t \in \mathcal{A}$ and the reward $\mathcal{R}$, based on state $s \in \mathcal{S}$. The training goal is maximizing the reward expectation $\mathbf{E}(\sum_{t=1}^{T} \gamma^{t-1} r^t)$.

Transition. IsaacGym (Makoviychuk et al., 2021) is adopted for simulation. A 24-joint humanoid with SMPL (Loper et al., 2015) kinematics and physical properties following Luo et al. (2021; 2023) is adopted with variable shape parameter $\beta \in \mathbb{R}^{10}$. Thus, a human pose at timestamp t could be defined as $q^t = \{\theta^t, p^t\}$, where $\theta^t \in \mathbb{R}^{J\times 6}$ is the joint rotation in the 6d representation (Zhou et al., 2019) and $p^t \in \mathbb{R}^{J\times 3}$ is the 3D joint position.

State. At timestamp t, s^t contains the observed s_o^t and s_i^{t+1} to imitate. s_o^t is defined in simulator as $s_o^t = (q_t, \dot{q}_t, \beta)$ with 3D body pose q_t, velocity $\dot{q}_t$, and body shape β. s_i^{t+1} is defined similarly except that it is the reference motion with finite-differentiated velocities.

Action. All joints but the pelvis are actuated with proportional derivative (PD) controllers, with a^t as the PD target. The torque applied could be calculated as

$$\tau^t = k^p \circ (a^t - q^t) - k^d \circ \dot{q}^t. \tag{3}$$

Reward. The reward is composed of four terms: motion imitation reward for minimizing the difference between the imitated states and the expected states, fail-state recovery reward (Luo et al., 2023), AMP reward (Peng et al., 2021), and energy reward to reduce jittering.

Training. Following PHC, three primitive policies are progressively trained with hard negative mining, two for pure motion imitation, and one for fail-state recovery. Then, a composer learns to combine the primitives dynamically. PPO (Schulman et al., 2017) is adopted to train the policies.

3.2 Imitated Data Acquisition

With the imitator π, we pursue to extract its inherent ID knowledge. As in Eq. 2, though the imitator-produced τ is not accurate for $s_o^t \rightarrow s_i^{t+1}$ since s_i^{t+1} is not guaranteed to reach, τ is accurate for

Table 1: ImDy compared to related human dynamics datasets. Zell et al. (2020) recorded full-body data but simplified the upper body with a single torso segment. All previous efforts contain only GRF for feet (indicated with *), while we include full body GRF.

Dataset	#Subj	Duration (h)	Dynamics	Body Repr.	Style
Zell et al. (2020)	22	0.07	GRF* & Torques	Partial Skeleton*	Real
Scott et al. (2020)	10	7.6	vertical GRF*	Skeleton	Real
UnderPressure (Mourot et al., 2022)	10	5.5	vertical GRF*	Skeleton	Real
GroundLink (Han et al., 2023)	7	1.5	GRF*	**SMPL**	Real
AddBiomechanics (Werling et al., 2024)	273	57.6	GRF* & Torques	Rajagopal et al. (2016)	Real
ImDy	**435**	**152.3**	**GRF & Torques**	**SMPL**	Simulated

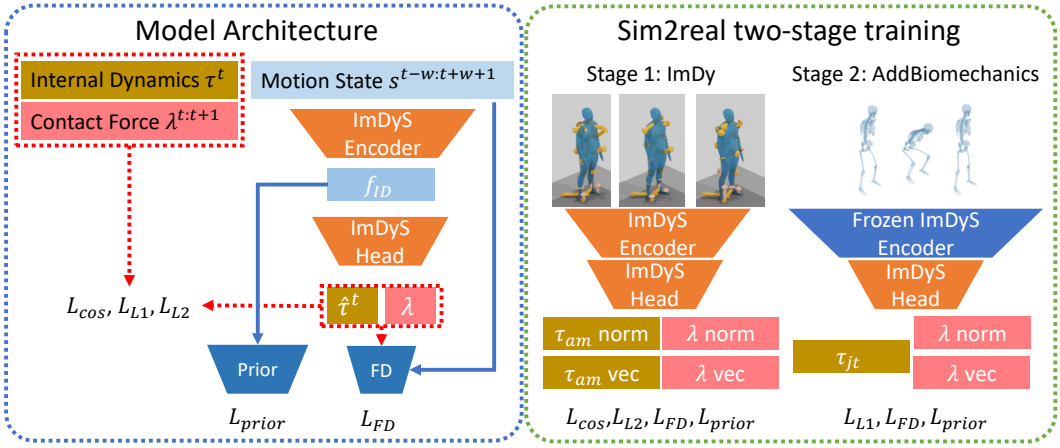

Figure 3: ImDyS overview. Taking a motion transition, ImDyS predicts the internal dynamics and ground reaction forces. Moreover, a prior discriminator is trained with the feature from ImDyS. A two-stage sim2real training curriculum is further designed.

$s_o^t \rightarrow s_o^{t+1}$. Thus, the idea could be as simple as using π to imitate arbitrary motions in the simulator, then collecting all the **observed** states s_o, the applied torques τ, and the full-body GRF λ.

We adopt AMASS (Mahmood et al., 2019) and KIT (Mandery et al., 2016) as two major data sources. Sequences involving humans interacting with objects other than the ground are excluded, resulting in over 50 hours of motion. All the sequences are re-sampled to 30FPS, with the z-axis as the gravity axis. Then, the sequences are imitated three times by the two primitive policies and the multiplicative policy with a simulation frequency of 60Hz, resulting in over 150 hours of human motion data with dynamics. States including $q, \dot{q}, \beta$ are recorded in synchronous with the torque τ, all restored in the format of SMPL (Loper et al., 2015) if possible. Moreover, GRFs for the whole body are also recorded, resulting in ImDy, a large-scale human motion dynamics dataset.

Detailed statistics of ImDy are demonstrated in Tab. 1. There are three major advantages. First, a considerably larger data scale is **100**$\times$ compared to previous efforts with full-body dynamics data, covering a wide span of human motion, which could be hard to acquire in laboratory setups. Second, thanks to the advanced simulator (Makoviychuk et al., 2021), we could include ground reaction forces for the whole body instead of the two feet only like in previous efforts. Finally, we represent humans with SMPL (Loper et al., 2015), increasing availability.

4 Learning ImDyS

With the collected ImDy, we could address the human inverse dynamics in a full-supervised manner with a data-driven solver ImDyS. In Sec. 4.1, we first introduce the formulation of data-driven inverse dynamics. Then, the proposed data-driven solver is introduced in Sec. 4.2. The overall pipeline of ImDyS is illustrated in Fig. 3.

4.1 FORMULATION

Recall the abstraction of ID in Eq. 2, which we rewrite as

$$(\tau^t, \lambda^{t:t+1}) = ImDyS(s^{t-w:t+w+1}). \tag{4}$$

Given the kinematics states from timestamp $t-w$ to $t+w+1$, ImDyS is required to estimate the internal dynamics τ^t for the transition from s^t to s^{t+1} and the ground reaction forces λ that the subject bears in timestamp t and $t+1$.

Motion States s could be represented by either SMPL parameters, joint angles, joint coordinates, or marker coordinates. However, due to the topology divergence, the conversion among SMPL parameters, joint angles, and joint coordinates is non-trivial with limited performances. To guarantee that ImDyS could be seamlessly adopted to both ImDy and real-world biomechanics data, we adopt marker coordinates as motion state representation for ImDyS. The state $s^t = (m^t, \dot{m}^t)$ is composed of marker coordinates m^t and finite-differentiated velocities $\dot{m}^t$ at timestamp t, which are easy to obtain for both ImDy and AddBiomechanics (Werling et al., 2024). Two temporal windows before and after the transition with a length of w are included for contextual information. Notice that human physical properties like height and weight could also be implicitly represented by the markers. The states are canonicalized w.r.t. the heading direction of s^t.

Internal Dynamics τ. For ImDy, the imposed angular momentum τ_{am} is adopted for dynamics representation. Notice that in Sec. 3.2, the original sequences are in 30FPS, while the simulation runs at 60FPS. This means for each motion transition (s^t, s^{t+1}), two torques were applied sequentially, each for $\frac{1}{60}s$. Predicting both torques is a plausible design choice. However, the second torque is based on the un-recorded mid-state between s^t, s^{t+1}. Predicting it involves the forward dynamics from s^t to the mid-state, with increased complexity. To this end, instead of predicting instantaneous torques, we switch to predicting the imposed angular momentum $\tau_{am} \in \mathbb{R}^{(J-1)\times 3}$, the time-accumulation effect of torque, for each motion transition. Thus, the modeling could stay consistent with proper complexity, only needing to sum the two torques up for s^t, s^{t+1} and then multiply it with the delta time. For AddBiomechanics, joint torque τ_{jt} is adopted for dynamics representation.

Ground Reaction Forces λ**.** Different from previous efforts (Mourot et al., 2022; Han et al., 2023; Werling et al., 2024) with foot GRFs only, we predict full-body GRF $\lambda \in \mathbb{R}^{J\times 3}$ as in Fig. 1.

4.2 DATA-DRIVEN IMDYS

Model architecture. With the enormous data scale of ImDy, we would like to keep ImDyS simple. An encoder-head structure is adopted. $s^{t-w:t+w+1} \in \mathbb{R}^{M\times(2w+2)\times 6}$ is first flattened as $\tilde{s}^{t-w:t+w+1} \in \mathbb{R}^{M\times(12w+12)}$ with window size w and M markers. Then, a transformer encoder converts $\tilde{s}$ into ID feature $f_{ID} \in \mathbb{R}^d$, where d is the feature dimension. For prediction, we decompose τ_{am} and λ into magnitudes $|\tau^t_{am}|, |\lambda^{t:t+1}|$ and direction vectors $\vec{\tau}^t_{am}, \vec{\lambda}^{t:t+1}$ and predict each of them with a linear head. τ^t_{jt} is predicted with another linear head. The final predictions are $\hat{\tau}^t_{am} = |\tau^t_{am}|\vec{\tau}^t_{am}, \hat{\lambda}^{t:t+1} = |\lambda^{t:t+1}|\vec{\lambda}^{t:t+1}$ and τ^t_{jt}.

Loss terms. L1 loss, cosine loss, and L2 loss are adopted to optimized the predicted magnitudes $|\tau^t_{am}|, |\lambda^{t:t+1}|$, direction vectors $\vec{\tau}^t_{am}, \vec{\lambda}^{t:t+1}$, and joint torques τ_{jt} as L_{mag}, L_{cos}, L_{L2} respectively. Besides, a forward dynamics (FD) loss L_{fd} is proposed with an auxiliary FD model to inform the learning with the ID-FD cycle. The FD model takes $s^{t-w:t}, \tau^t = (\tau^t_{am}, \tau^t_{jt}), \lambda^t$ as input, predicts the next-frame joint angles. The FD loss is thus computed with cycle consistency as

$$L_{FD} = |s^{t+1} - FD(s^{t-w:t}, \hat{\tau}^t, \hat{\lambda}^t)|. \tag{5}$$

Finally, we devise a loss term similar to Peng et al. (2021), which encourages the ImDy feature f_{ID} to model physically plausible motion transitions. A linear discriminator takes f_{ID} and outputs a logit indicating whether the motion transition is plausible. To train the discriminator, besides the positive samples from ImDy and AMASS (Mahmood et al., 2019), we propose two negative sample generation strategies. First, $s^{t-w:t+w+1}$ is randomly permuted along the temporal axis. Second, random Gaussian noises are added on $s^{t-w:t+w+1}$. Binary cross-entropy loss is adopted as L_{cls}.

Sim2Real training curriculum is devised in a simple two-stage manner. In the first stage, ImDyS is trained on ImDy, with the overall loss as $\mathcal{L}_{s1} = \alpha_1 L_{mag} + \alpha_2 L_{cos} + \alpha_3 L_{FD} + \alpha_4 L_{cls}$. In the second

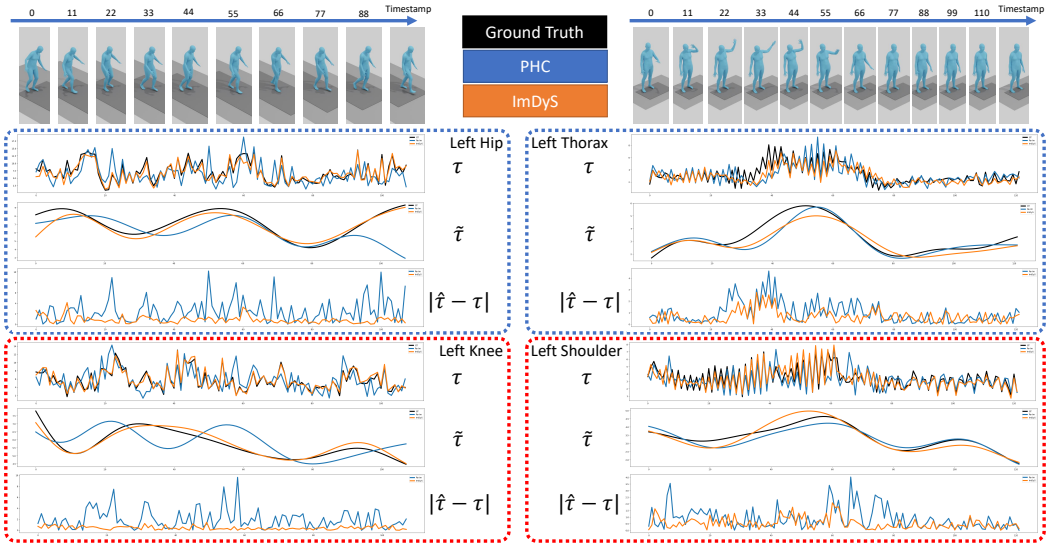

Figure 4: Qualitative results on ImDy. ˜ indicates a low-pass filter at 14Hz is applied. A typical gait sample and an arm-waving sample are visualized.

stage, we freeze the encoder and train the linear head for joint torques τ_{jt}. The loss is calculated as $\mathcal{L}_{s2} = \alpha_3 L_{FD} + \alpha_4 L_{cls} + \alpha_5 L_{L2}$. Results show that ImDy pre-trained encoder converges fast on AddBiomechanics, indicating that it holds useful knowledge on real-world human dynamics.

5 Experiments

5.1 Implementation Details

PHC (Luo et al., 2023) adopted the position-control mode implemented by IsaacGym (Makoviychuk et al., 2021), where the imposed torque is calculated differently from the naive PD controller and inaccessible. Therefore, we re-trained the PHC on AMASS (Mahmood et al., 2019) with the effort-control mode, and a naive PD controller was adopted. Training the PHC took approximately 10 days, with a success rate on AMASS of 91.3%. The window size w is set as 2 to keep a short-term motion modeling, which is proven helpful in Sec. 5.3. The encoder of ImDyS is a three-layer transformer with a dimension of 64, ReLU activation, and LayerNorm. The loss weights are set as $\alpha_1 = \alpha_3 = 0.01$, $\alpha_2 = \alpha_4 = \alpha_5 = 1$ to maintain all terms at similar numerical scales for training stability. ImDyS, the prior discriminator, and the FD model are all trained using the AdamW optimizer with a batch size of 2,400 for 140 epochs on ImDy for the first stage. For the second stage, ImDyS is further tuned on AddBiomechanics for only 10 epochs with the same hyper-parameters. When generating negative samples for the prior discriminator, the two strategies are randomly adopted with a positive-negative ratio of 1:1. We split ImDy into a training set of 27,501 sequences and a test set of 3,055 sequences. All the data collection processes and experiments are conducted on a single NVIDIA RTX3090 GPU.

5.2 Evaluation on ImDy

Metric. We calculate the mPJE (mean Per Joint Error) for τ and λ as

$$mPJE_{\tau} = \frac{1}{J}\sum_{j=1}^{J} |\tau_j - \hat{\tau}_j|_2,\ mPJE_{\lambda} = \frac{1}{J}\sum_{j=1}^{J} |\lambda_j - \hat{\lambda}_j|_2, \tag{6}$$

where J is the number of joints. The result is further normalized by body weight to align different subjects, with units of $N \cdot m \cdot s/kg$ and N/kg. Specifically, the mPJE for the GRF on both feet $mPJE_{\lambda_{lf}}, mPJE_{\lambda_{rf}}$ is also reported.

Baseline. Few efforts except IL algorithms are feasible as baselines. To this end, we introduce PHC as a baseline, where the sequences in ImDy are re-imitated by the re-trained PHC. The imposed

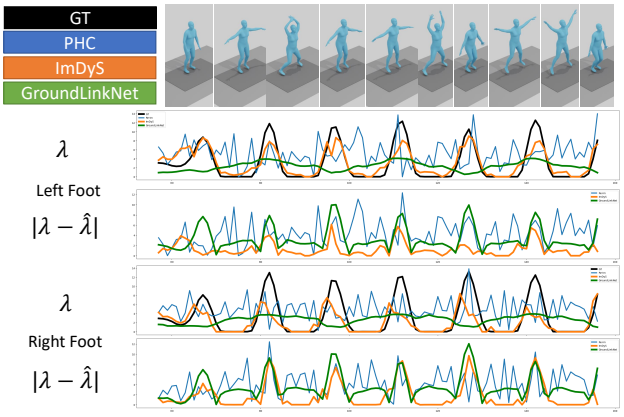

Figure 5: Qualitative results on GroundLink including PHC, GroundLinkNet, and ImDyS. The GRF λ for both feet are shown. Surprisingly, ImDyS provides better consistency with the ground truth.

Table 2: Quantitative results on ImDy. mPJE is normalized by the body weight.

Methods	PHC	ImDyS
$mPJE_{\tau}$ $(Nms/kg)\downarrow$	0.095	**0.021**
$mPJE_{\lambda}$ $(N/kg)\downarrow$	0.409	**0.289**
$mPJE_{\lambda_{lf}}$ $(N/kg)\downarrow$	3.034	**1.843**
$mPJE_{\lambda_{rf}}$ $(N/kg)\downarrow$	2.866	**1.842**

Table 3: Ground reaction force prediction results on GroundLink.

Methods	PHC	GroundLinkNet	ImDyS
$mPJE_{\lambda_{lf}}$ $(N/kg)\downarrow$	2.362	5.423	**0.986**
$mPJE_{\lambda_{rf}}$ $(N/kg)\downarrow$	2.636	2.891	**1.149**

Table 4: Quantitative results on AddBiomechanics.

Methods	Baseline (150 epochs)	ImDyS (10 epochs)
$mPJE_{\tau}$ $(Nm/kg)\downarrow$	0.1699	**0.1626**$_{\downarrow 4.30\%}$
$mPJE_{\lambda}$ $(Nm/kg)\downarrow$	1.0876	**1.0633**$_{\downarrow 2.18\%}$

angular momentums and the GRF obtained via the re-imitation process are adopted as the baseline predictions. With this baseline, we demonstrate the amplification effect from the kinematics error to the dynamics error, thus validating the performance of directly adopting IL for ID.

Results. Quantitative results are shown in Tab. 2. PHC produces an mPJPE of 56.13 mm, which is admirable for kinematics but results in high dynamics errors. ImDyS demonstrates considerably better performance. We further visualize two qualitative samples in Fig. 4. Since the raw data could be jittering, we also filter the predictions with a low-pass filter at 14Hz, denoted as $\tilde{\tau}, \tilde{\lambda}$, which helps reveal the general trend of the predictions. For the gait sample at the left, the imposed angular momentum τ at the left hip and the left knee are plotted, along with the GRF λ at the left toe. We also plot the error between the predicted values and GT values. ImDyS manages to faithfully reconstruct τ for the left knee and hip with minor errors. Meanwhile, PHC typically produces higher errors due to phase mismatch. As shown, it tends to lag behind the input motion. For GRF, ImDyS also produces reasonable predictions. Besides a typical gait analysis sample, we also demonstrate the performance of ImDyS with an arm-waving motion. The τ at directly related body segments including the left thorax and shoulder is visualized. ImDyS reproduces the dynamic status with better alignment to GT compared to PHC. Generally, ImDyS produces reasonable ID predictions. A potential issue is the jittering prediction, which is a consequence of the jittering observations in ImDy. However, we show that ImDyS could handle real-world smooth observations well even when trained only on jittering ImDyS. More demonstrations are available in the supplementary video.

5.3 Evaluation on GroundLink

Metrics. GroundLink (Han et al., 2023) provides 1.5-hour motion from 7 subjects with GRF. We adopt subject 7 for evaluation. mPJE$_{\lambda}$ at both feet normalized by body weight is reported.

Baselines. PHC is evaluated similarly to Sec. 5.2. We also report the performance of GroundLinkNet (Han et al., 2023). PHC and ImDyS are not exposed to GroundLink during training, resulting in a **zero-shot** evaluation for ImDyS and the PHC baseline. Also, GroundLinkNet operates on 250FPS motion, while ImDyS and the PHC re-imitation baseline only operate on 30FPS motion. Finally, GroundLinkNet predicts GRF for both feet, while ImDyS and PHC could decouple feet into ankles and toes, and predict GRF separately for each part. We add up the ankle GRF and the toe GRF as the foot GRF. All predictions are re-sampled to 30FPS.

Results. Quantitative results are illustrated in Tab. 3. Surprisingly, both ImDyS and PHC manage to outperform the specifically trained GroundLinkNet. We attribute this to the enormous scale of AMASS and ImDy, which is much larger than GroundLink. Moreover, even though ImDyS is trained on simulated ImDy only, it generalizes to real-world data with competitive performance. We visualize the results in Fig. 5, 7. The PHC re-imitation baseline produces jittering predictions

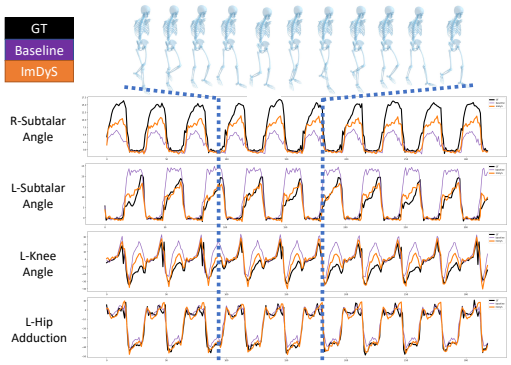

Figure 6: Joint torque predictions on AddBiomechanics.

Table 5: Ablation study on ImDy.

Methods	$mPJE_{\tau}$ $(Nms/kg)\downarrow$	$mPJE_{\lambda}$ $(N/kg)\downarrow$	$mPJE_{\lambda_{lf}}$ $(N/kg)\downarrow$	$mPJE_{\lambda_{rf}}$ $(N/kg)\downarrow$
ImDyS	0.021	0.289	1.843	1.842
ImDyS-SMPL	0.011	0.272	1.746	1.764
ImDyS-Joint	0.014	0.273	1.755	1.775
w/o L_{FD}	0.023	0.302	1.962	1.976
w/o L_{cls}	0.022	0.294	1.884	1.891

Table 6: Ablation study on AddBiomechanics.

Methods	ImDyS w=2	ImDyS w=1	ImDyS w=3
$mPJE_{\tau}$ $(Nm/kg)\downarrow$	**0.1626**	0.1690	0.1720
$mPJE_{\lambda}$ $(Nm/kg)\downarrow$	**1.0633**	1.0990	1.1030

similar to Fig. 4. GroundLinkNet, though specifically trained on GroundLink, fails to capture the rapid GRF changes in this jumping jack motion, resulting in a relatively flat output. In contrast, ImDyS surprisingly presents good consistency with GT, and even faithfully reproduces the intense peak GRFs for the left foot for the jumping jack. Besides, the prediction is not as jittering as in Fig. 4, indicating ImDyS could handle real-world smooth data well.

5.4 Evaluation on AddBiomechanics

Metrics. AddBiomechanics (Werling et al., 2024) is recently proposed with over 50 hours of human dynamics data from 273 subjects. We adopt the armless part of this dataset. We follow the train/test split in Addbiomechanics and report mPJE for the joint torque normalized by body weight.

Results. A baseline model trained only on AddBiomechanics for 150 epochs with the same architecture as ImDyS is reported to showcase the generalization from ImDy to real-world dynamics. All data are re-sampled to 30 FPS. Quantitative results are illustrated in Tab. 4. ImDyS outperforms the baseline with faster convergence, indicating the efficacy of Imdys in pre-training and mitigating the sim2real gap. Qualitative results are shown in Fig. 6, 8, where ImDyS shows better alignment with GT and more precise magnitude predictions. More analyses on the relationship between performance, data distribution and quality are in the appendix.

5.5 Ablation Studies

Different Motion Representations are evaluated on ImDy in Tab. 5. Though SMPL and joint-based representations perform better, we adopt marker-based representation for its generality.

Different Loss Terms are evaluated in Tab. 5. L_{FD} is proven to contribute more than L_{cls}.

Different Window Sizes w are evaluated on AddBiomechanics in Tab. 6. ImDyS achieves the best balance between rich contexts and conciseness with $w = 2$.

6 Discussion

Given the fully simulated nature of ImDy, a reasonable question is the sim2real problem. ImDy could be unnaturally jittering as in Fig. 4. Also, the physical properties of the simulated humanoid differ from those of real humans. Empirically, experiments show that ImDyS generalizes well to real-world data, partially mitigating this gap. The reason could be threefold. First, the jitters are unnatural but still physically plausible given that ImDy faithfully preserves consistent information for the simulated physics phenomena. Second, the small window size of ImDyS prevents it from relying on long-term contexts, where jitters are more salient. Finally, the enormous scale of ImDy is helpful for generalization. To further mitigate the sim2real gap with ImDy is a meaningful goal to pursue. Besides, ImDyS is designed as a first-step baseline to demonstrate the efficacy of ImDy. Introducing more sophisticated designs to regulate the behavior of ImDyS would be preferable.

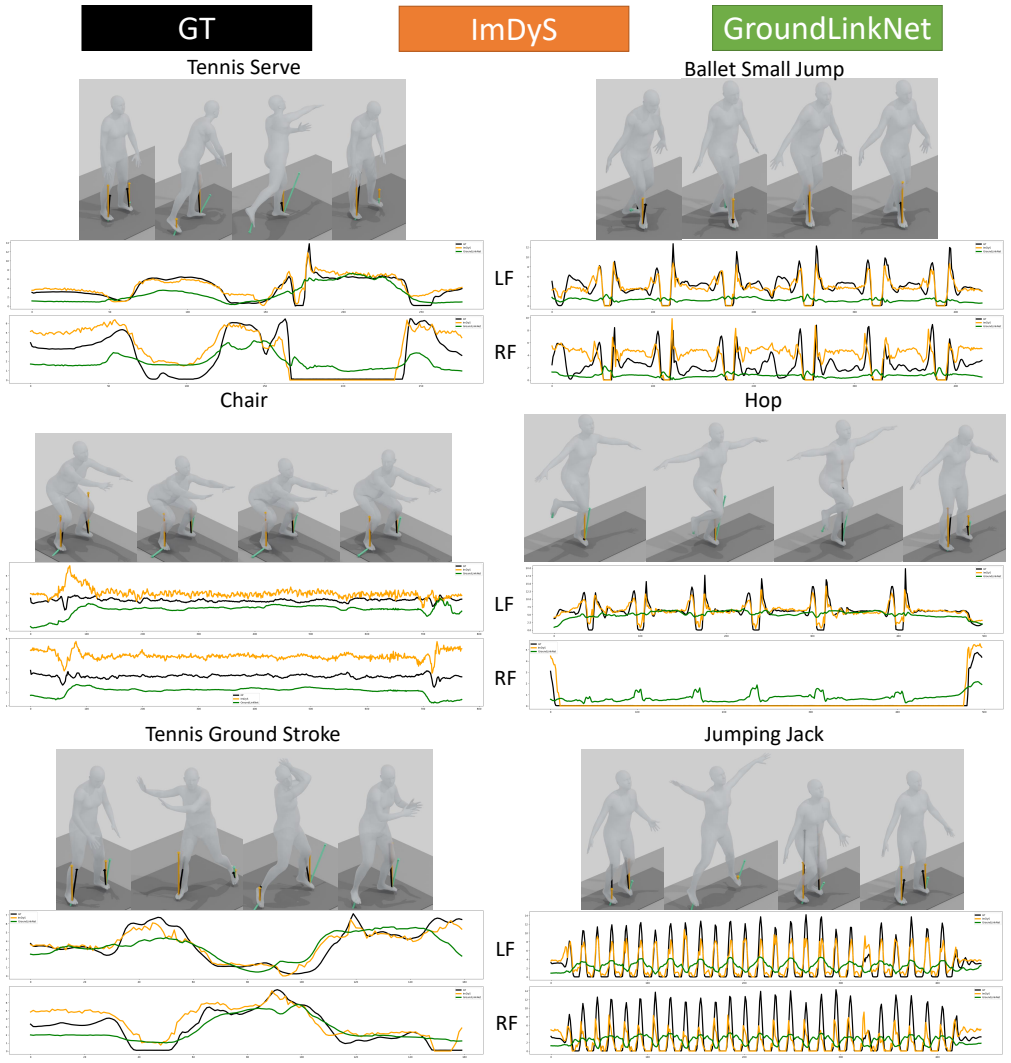

Figure 7: Extensive visualization on GroundLink. For various motions, ImDyS shows superior alignment with GT compared to specifically trained GroundLinkNet, showcasing the efficacy of ImDy. Especially, the intense peaks are also reproduced by ImDyS.

Moreover, ImDy only considers GRF, while other external forces are not involved. Also, interaction with other entities is absent. Exploration of these would be interesting for future works.

7 Conclusion

Leveraging the inherent resemblance between inverse dynamics and imitation learning, we proposed a novel human dynamics dataset ImDy, which contained over 150 hours of human motion paired with full-body driven torques and GRFs from well-developed simulator and imitation algorithms. Based on ImDy, a data-driven human inverse dynamics solver ImDyS is devised to reconstruct the driven angular momentum and contact forces from kinematic observations. ImDyS demonstrated impressive performance on both simulated and real-world data. As a first step toward scalable and easily accessible human inverse dynamics, we hope ImDy can shed new light on the data-driven physical analysis of human motion.

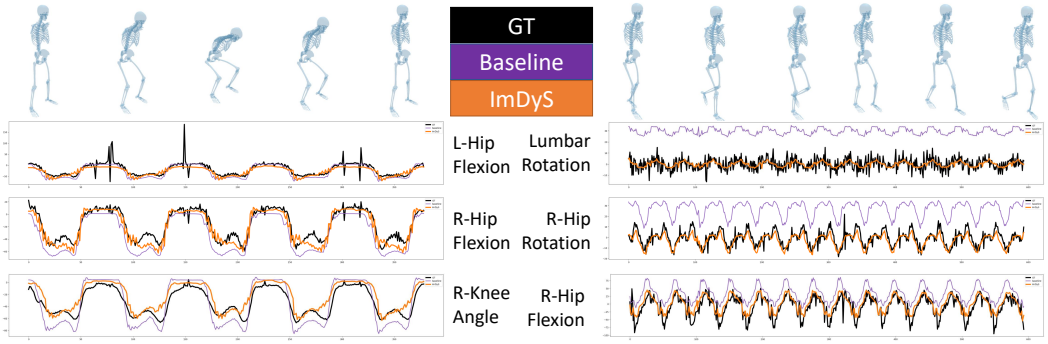

Figure 8: Extensive visualization on AddBiomechanics. ImDyS demonstrates superior performance to the baseline, indicating ImDy's generalization ability.

REFERENCES

Kevin Bergamin, Simon Clavet, Daniel Holden, and James Richard Forbes. Drecon: data-driven responsive control of physics-based characters. *ACM Transactions On Graphics (TOG)*, 38(6): 1–11, 2019.

Michael Damsgaard, John Rasmussen, Søren Tørholm Christensen, Egidijus Surma, and Mark De Zee. Analysis of musculoskeletal systems in the anybody modeling system. *Simulation Modelling Practice and Theory*, 14(8):1100–1111, 2006.

Scott L Delp, Frank C Anderson, Allison S Arnold, Peter Loan, Ayman Habib, Chand T John, Eran Guendelman, and Darryl G Thelen. Opensim: open-source software to create and analyze dynamic simulations of movement. *IEEE transactions on biomedical engineering*, 54(11):1940–1950, 2007.

Claudiane A Fukuchi, Reginaldo K Fukuchi, and Marcos Duarte. A public dataset of overground and treadmill walking kinematics and kinetics in healthy individuals. *PeerJ*, 6:e4640, 2018.

E. Gartner, M. Andriluka, E. Coumans, and C. Sminchisescu. Differentiable dynamics for articulated 3d human motion reconstruction. In *2022 IEEE/CVF Conference on Computer Vision and Pattern Recognition (CVPR)*, pp. 13180–13190, Los Alamitos, CA, USA, jun 2022. IEEE Computer Society. doi: 10.1109/CVPR52688.2022.01284. URL https://doi.ieeecomputersociety.org/10.1109/CVPR52688.2022.01284.

Chuan Guo, Shihao Zou, Xinxin Zuo, Sen Wang, Wei Ji, Xingyu Li, and Li Cheng. Generating diverse and natural 3d human motions from text. In *2022 IEEE/CVF Conference on Computer Vision and Pattern Recognition (CVPR)*, pp. 5142–5151, Los Alamitos, CA, USA, 2022. IEEE Computer Society. doi: 10.1109/CVPR52688.2022.00509.

Erik Gärtner, Mykhaylo Andriluka, Hongyi Xu, and Cristian Sminchisescu. Trajectory optimization for physics-based reconstruction of 3d human pose from monocular video. In *2022 IEEE/CVF Conference on Computer Vision and Pattern Recognition (CVPR)*, pp. 13096–13105, Los Alamitos, CA, USA, 2022. IEEE Computer Society. doi: 10.1109/CVPR52688.2022.01276.

Xingjian Han, Ben Senderling, Stanley To, Deepak Kumar, Emily Whiting, and Jun Saito. Groundlink: A dataset unifying human body movement and ground reaction dynamics. In *SIGGRAPH Asia 2023 Conference Papers*, SA '23, New York, NY, USA, 2023. Association for Computing Machinery. ISBN 9798400703157. doi: 10.1145/3610548.3618247. URL https://doi.org/10.1145/3610548.3618247.

B. Huang, L. Pan, Y. Yang, J. Ju, and Y. Wang. Neural mocon: Neural motion control for physically plausible human motion capture. In *2022 IEEE/CVF Conference on Computer Vision and Pattern Recognition (CVPR)*, pp. 6407–6416, Los Alamitos, CA, USA, jun 2022. IEEE Computer Society. doi: 10.1109/CVPR52688.2022.00631. URL https://doi.ieeecomputersociety.org/10.1109/CVPR52688.2022.00631.

Leif Johnson and Dana H. Ballard. Efficient codes for inverse dynamics during walking. In Carla E. Brodley and Peter Stone (eds.), *Proceedings of the Twenty-Eighth AAAI Conference on Artificial Intelligence*, pp. 343–349, Québec City, Québec, Canada, 2014. AAAI Press. doi: 10.1609/AAAI.V28I1.8747. URL https://doi.org/10.1609/aaai.v28i1.8747.

Marilyn Keller, Keenon Werling, Soyong Shin, Scott Delp, Sergi Pujades, C Karen Liu, and Michael J Black. From skin to skeleton: Towards biomechanically accurate 3d digital humans. *ACM Transactions on Graphics (TOG)*, 42(6):1–12, 2023.

Claudia Latella, Naveen Kuppuswamy, Francesco Romano, Silvio Traversaro, and Francesco Nori. Whole-body human inverse dynamics with distributed micro-accelerometers, gyros and force sensing. *Sensors*, 16(5), 2016. ISSN 1424-8220. doi: 10.3390/s16050727. URL https://www.mdpi.com/1424-8220/16/5/727.

Claudia Latella, Silvio Traversaro, Diego Ferigo, Yeshasvi Tirupachuri, Lorenzo Rapetti, Francisco Javier Andrade Chavez, Francesco Nori, and Daniele Pucci. Simultaneous floating-base estimation of human kinematics and joint torques. *Sensors*, 19(12), 2019. ISSN 1424-8220. doi: 10.3390/s19122794. URL https://www.mdpi.com/1424-8220/19/12/2794.

Jiefeng Li, Siyuan Bian, Chao Xu, Gang Liu, Gang Yu, and Cewu Lu. D &d: Learning human dynamics from dynamic camera. In *Computer Vision – ECCV 2022: 17th European Conference, Tel Aviv, Israel, October 23–27, 2022, Proceedings, Part V*, pp. 479–496, Berlin, Heidelberg, 2022. Springer-Verlag. ISBN 978-3-031-20064-9. doi: 10.1007/978-3-031-20065-6_28. URL https://doi.org/10.1007/978-3-031-20065-6_28.

Matthew Loper, Naureen Mahmood, Javier Romero, Gerard Pons-Moll, and Michael J. Black. Smpl: a skinned multi-person linear model. In *ACM Transactions on Graphics*, volume 34, New York, NY, USA, oct 2015. Association for Computing Machinery. doi: 10.1145/2816795.2818013. URL https://doi.org/10.1145/2816795.2818013.

Z. Luo, J. Cao, A. Winkler, K. Kitani, and W. Xu. Perpetual humanoid control for real-time simulated avatars. In *2023 IEEE/CVF International Conference on Computer Vision (ICCV)*, pp. 10861–10870, Los Alamitos, CA, USA, oct 2023. IEEE Computer Society. doi: 10.1109/ICCV51070.2023.01000. URL https://doi.ieeecomputersociety.org/10.1109/ICCV51070.2023.01000.

Zhengyi Luo, Ryo Hachiuma, Ye Yuan, and Kris Kitani. Dynamics-regulated kinematic policy for egocentric pose estimation. *Advances in Neural Information Processing Systems*, 34:25019–25032, 2021.

Xiaolei Lv, Jinxiang Chai, and Shihong Xia. Data-driven inverse dynamics for human motion. *ACM Transactions on Graphics (TOG)*, 35(6):1–12, 2016.

N. Mahmood, N. Ghorbani, N. F. Troje, G. Pons-Moll, and M. Black. Amass: Archive of motion capture as surface shapes. In *2019 IEEE/CVF International Conference on Computer Vision (ICCV)*, pp. 5441–5450, Los Alamitos, CA, USA, nov 2019. IEEE Computer Society. doi: 10.1109/ICCV.2019.00554. URL https://doi.ieeecomputersociety.org/10.1109/ICCV.2019.00554.

Viktor Makoviychuk, Lukasz Wawrzyniak, Yunrong Guo, Michelle Lu, Kier Storey, Miles Macklin, David Hoeller, Nikita Rudin, Arthur Allshire, Ankur Handa, and Gavriel State. Isaac gym: High performance GPU based physics simulation for robot learning. In Joaquin Vanschoren and Sai-Kit Yeung (eds.), *Proceedings of the Neural Information Processing Systems Track on Datasets and Benchmarks*, Virtual, 2021. Curran Associates Inc. URL https://datasets-benchmarks-proceedings.neurips.cc/paper/2021/hash/28dd2c7955ce926456240b2ff0100bde-Abstract-round2.html.

Christian Mandery, Ömer Terlemez, Martin Do, Nikolaus Vahrenkamp, and Tamim Asfour. Unifying representations and large-scale whole-body motion databases for studying human motion. *IEEE Transactions on Robotics*, 32(4):796–809, 2016.

Mykhailo Manukian, Serhii Bahdasariants, and Sergiy Yakovenko. Artificial physics engine for real-time inverse dynamics of arm and hand movement. *Plos one*, 18(12):e0295750, 2023.

Lucas Mourot, Ludovic Hoyet, François Le Clerc, and Pierre Hellier. Underpressure: Deep learning for foot contact detection, ground reaction force estimation and footskate cleanup. *Computer Graphics Forum*, 41(8):195–206, 2022. doi: https://doi.org/10.1111/cgf.14635. URL https://onlinelibrary.wiley.com/doi/abs/10.1111/cgf.14635.

Xue Bin Peng, Ze Ma, Pieter Abbeel, Sergey Levine, and Angjoo Kanazawa. Amp: Adversarial motion priors for stylized physics-based character control. *ACM Transactions on Graphics (ToG)*, 40(4):1–20, 2021.

Xue Bin Peng, Yunrong Guo, Lina Halper, Sergey Levine, and Sanja Fidler. Ase: Large-scale reusable adversarial skill embeddings for physically simulated characters. *ACM Transactions On Graphics (TOG)*, 41(4):1–17, 2022.

A. R. Punnakkal, A. Chandrasekaran, N. Athanasiou, A. Quiros-Ramirez, and M. J. Black. Babel: Bodies, action and behavior with english labels. In *2021 IEEE/CVF Conference on Computer Vision and Pattern Recognition (CVPR)*, pp. 722–731, Los Alamitos, CA, USA, jun 2021. IEEE Computer Society. doi: 10.1109/CVPR46437.2021.00078. URL https://doi.ieeecomputersociety.org/10.1109/CVPR46437.2021.00078.

Apoorva Rajagopal, Christopher L Dembia, Matthew S DeMers, Denny D Delp, Jennifer L Hicks, and Scott L Delp. Full-body musculoskeletal model for muscle-driven simulation of human gait. *IEEE transactions on biomedical engineering*, 63(10):2068–2079, 2016.

Davis Rempe, Leonidas J. Guibas, Aaron Hertzmann, Bryan Russell, Ruben Villegas, and Jimei Yang. Contact and human dynamics from monocular video. In *Computer Vision – ECCV 2020: 16th European Conference, Glasgow, UK, August 23–28, 2020, Proceedings, Part V*, pp. 71–87, Berlin, Heidelberg, 2020. Springer-Verlag. ISBN 978-3-030-58557-0. doi: 10.1007/978-3-030-58558-7_5. URL https://doi.org/10.1007/978-3-030-58558-7_5.

Céline Schreiber and Florent Moissenet. A multimodal dataset of human gait at different walking speeds established on injury-free adult participants. *Scientific data*, 6(1):111, 2019.

John Schulman, Filip Wolski, Prafulla Dhariwal, Alec Radford, and Oleg Klimov. Proximal policy optimization algorithms. preprint on webpage at arXiv:1707.06347, 2017.

Jesse Scott, Bharadwaj Ravichandran, Christopher Funk, Robert T. Collins, and Yanxi Liu. From image to stability: Learning dynamics from human pose. In *Computer Vision – ECCV 2020: 16th European Conference, Glasgow, UK, August 23–28, 2020, Proceedings, Part XXIII*, pp. 536–554, Berlin, Heidelberg, 2020. Springer-Verlag. ISBN 978-3-030-58591-4. doi: 10.1007/978-3-030-58592-1_32. URL https://doi.org/10.1007/978-3-030-58592-1_32.

A. Shahroudy, J. Liu, T. Ng, and G. Wang. Ntu rgb+d: A large scale dataset for 3d human activity analysis. In *2016 IEEE Conference on Computer Vision and Pattern Recognition (CVPR)*, pp. 1010–1019, Los Alamitos, CA, USA, jun 2016. IEEE Computer Society. doi: 10.1109/CVPR.2016.115. URL https://doi.ieeecomputersociety.org/10.1109/CVPR.2016.115.

Soshi Shimada, Vladislav Golyanik, Weipeng Xu, Patrick Pérez, and Christian Theobalt. Neural monocular 3d human motion capture with physical awareness. *ACM Transactions on Graphics (ToG)*, 40(4):1–15, 2021.

Guy Tevet, Sigal Raab, Brian Gordon, Yonatan Shafir, Daniel Cohen-Or, and Amit Haim Bermano. Human motion diffusion model. In *The Eleventh International Conference on Learning Representations ICLR 2023*, Kigali, Rwanda, 2023. OpenReview.net. URL https://openreview.net/pdf?id=SJ1kSyO2jwu.

Thomas K Uchida and Scott L Delp. *Biomechanics of movement: the science of sports, robotics, and rehabilitation*. Mit Press, 2021.

Thomas K Uchida and Ajay Seth. Conclusion or illusion: Quantifying uncertainty in inverse analyses from marker-based motion capture due to errors in marker registration and model scaling. *Frontiers in Bioengineering and Biotechnology*, 10:874725, 2022.

J. Wang, Y. Yuan, Z. Luo, K. Xie, D. Lin, U. Iqbal, S. Fidler, and S. Khamis. Learning human dynamics in autonomous driving scenarios. In *2023 IEEE/CVF International Conference on Computer Vision (ICCV)*, pp. 20739–20749, Los Alamitos, CA, USA, oct 2023. IEEE Computer Society. doi: 10.1109/ICCV51070.2023.01901. URL https://doi.ieeecomputersociety.org/10.1109/ICCV51070.2023.01901.

Keenon Werling, Dalton Omens, Jeongseok Lee, Ioannis Exarchos, and C. Karen Liu. Fast and Feature-Complete Differentiable Physics Engine for Articulated Rigid Bodies with Contact Constraints. In *Robotics: Science and Systems XVII, Virtual Event, July 12-16, 2021*, Virtual, July 2021. RSS Foundation. doi: 10.15607/RSS.2021.XVII.034. URL https://doi.org/10.15607/RSS.2021.XVII.034.

Keenon Werling, Nicholas A Bianco, Michael Raitor, Jon Stingel, Jennifer L Hicks, Steven H Collins, Scott L Delp, and C Karen Liu. Addbiomechanics: Automating model scaling, inverse kinematics, and inverse dynamics from human motion data through sequential optimization. *Plos one*, 18(11):e0295152, 2023.

Keenon Werling, Janelle Kaneda, Alan Tan, Rishi Agarwal, Six Skov, Tom Van Wouwe, Scott Uhlrich, Nicholas Bianco, Carmichael Ong, Antoine Falisse, et al. Addbiomechanics dataset: Capturing the physics of human motion at scale. *arXiv preprint arXiv:2406.18537*, 2024.

Jungdam Won, Deepak Gopinath, and Jessica Hodgins. Control strategies for physically simulated characters performing two-player competitive sports. *ACM Transactions on Graphics (TOG)*, 40 (4):1–11, 2021.

Jungdam Won, Deepak Gopinath, and Jessica Hodgins. Physics-based character controllers using conditional vaes. *ACM Transactions on Graphics (TOG)*, 41(4):1–12, 2022.

Baoping Xiong, Nianyin Zeng, Han Li, Yuan Yang, Yurong Li, Meilan Huang, Wuxiang Shi, Min Du, and Yudong Zhang. Intelligent prediction of human lower extremity joint moment: an artificial neural network approach. *Ieee Access*, 7:29973–29980, 2019.

X. Yi, Y. Zhou, M. Habermann, S. Shimada, V. Golyanik, C. Theobalt, and F. Xu. Physical inertial poser (pip): Physics-aware real-time human motion tracking from sparse inertial sensors. In *2022 IEEE/CVF Conference on Computer Vision and Pattern Recognition (CVPR)*, pp. 13157–13168, Los Alamitos, CA, USA, jun 2022. IEEE Computer Society. doi: 10.1109/CVPR52688.2022.01282. URL https://doi.ieeecomputersociety.org/10.1109/CVPR52688.2022.01282.

Y. Yuan and K. Kitani. Ego-pose estimation and forecasting as real-time pd control. In *2019 IEEE/CVF International Conference on Computer Vision (ICCV)*, pp. 10081–10091, Los Alamitos, CA, USA, nov 2019. IEEE Computer Society. doi: 10.1109/ICCV.2019.01018. URL https://doi.ieeecomputersociety.org/10.1109/ICCV.2019.01018.

P. Zell and B. Rosenhahn. Learning-based inverse dynamics of human motion. In *2017 IEEE International Conference on Computer Vision Workshop (ICCVW)*, pp. 842–850, Los Alamitos, CA, USA, oct 2017. IEEE Computer Society. doi: 10.1109/ICCVW.2017.104. URL https://doi.ieeecomputersociety.org/10.1109/ICCVW.2017.104.

P. Zell, B. Wandt, and B. Rosenhahn. Joint 3d human motion capture and physical analysis from monocular videos. In *2017 IEEE Conference on Computer Vision and Pattern Recognition Workshops (CVPRW)*, pp. 17–26, Los Alamitos, CA, USA, jul 2017. IEEE Computer Society. doi: 10.1109/CVPRW.2017.9. URL https://doi.ieeecomputersociety.org/10.1109/CVPRW.2017.9.

Petrissa Zell and Bodo Rosenhahn. A physics-based statistical model for human gait analysis. In Juergen Gall, Peter Gehler, and Bastian Leibe (eds.), *Pattern Recognition*, pp. 169–180, Cham, 2015. Springer International Publishing. ISBN 978-3-319-24947-6.

Petrissa Zell, Bodo Rosenhahn, and Bastian Wandt. Weakly-supervised learning of human dynamics. In Andrea Vedaldi, Horst Bischof, Thomas Brox, and Jan-Michael Frahm (eds.), *Computer Vision – ECCV 2020*, pp. 68–84, Cham, 2020. Springer International Publishing. ISBN 978-3-030-58574-7.

Y. Zhou, C. Barnes, J. Lu, J. Yang, and H. Li. On the continuity of rotation representations in neural networks. In *2019 IEEE/CVF Conference on Computer Vision and Pattern Recognition (CVPR)*, pp. 5738–5746, Los Alamitos, CA, USA, jun 2019. IEEE Computer Society. doi: 10.1109/CVPR.2019.00589. URL https://doi.ieeecomputersociety.org/10.1109/CVPR.2019.00589.

APPENDIX

A APPLICATIONS OF IMDYS

In this section, we demonstrate some downstream applications of ImDyS.

Human Work Analysis. With the predicted τ, we could calculate the work conducted at each joint. Visualizations are in Fig. 9, reasonably revealing the energy flow during human motion.

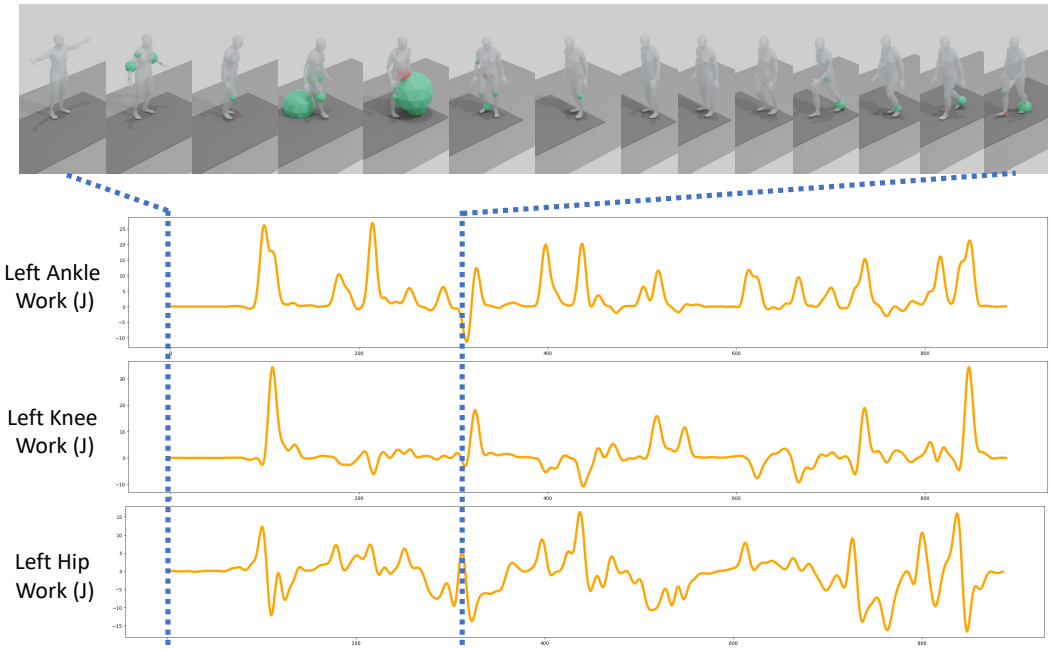

Figure 9: Human work visualization with ImDyS prediction. Green indicates positive work and red indicates negative work.

Motion Assessment. Another interesting application of ImDyS is based on the discriminator introduced in Sec. 4.2. Besides facilitating ImDyS learning, it could also assess whether a motion transition is physically plausible as in Fig. 10. Specifically, we adopt ImDyS to assess the motion generated from MDM Tevet et al. (2023). ImDyS reasonably tells when the motion starts to deviate from realism.

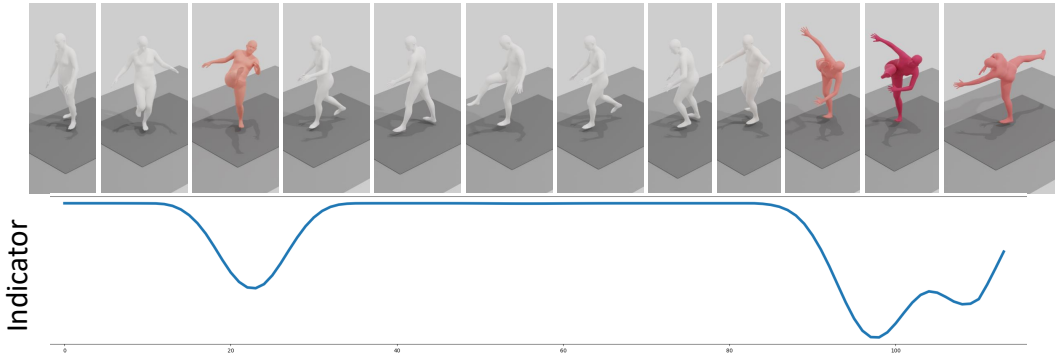

Figure 10: Motion assessment visualization. The motion artifacts are annotated with red with a low indicator value from ImDyS. As shown, ImDyS manages to identify implausible transitions in a kicking motion generated by MDM.

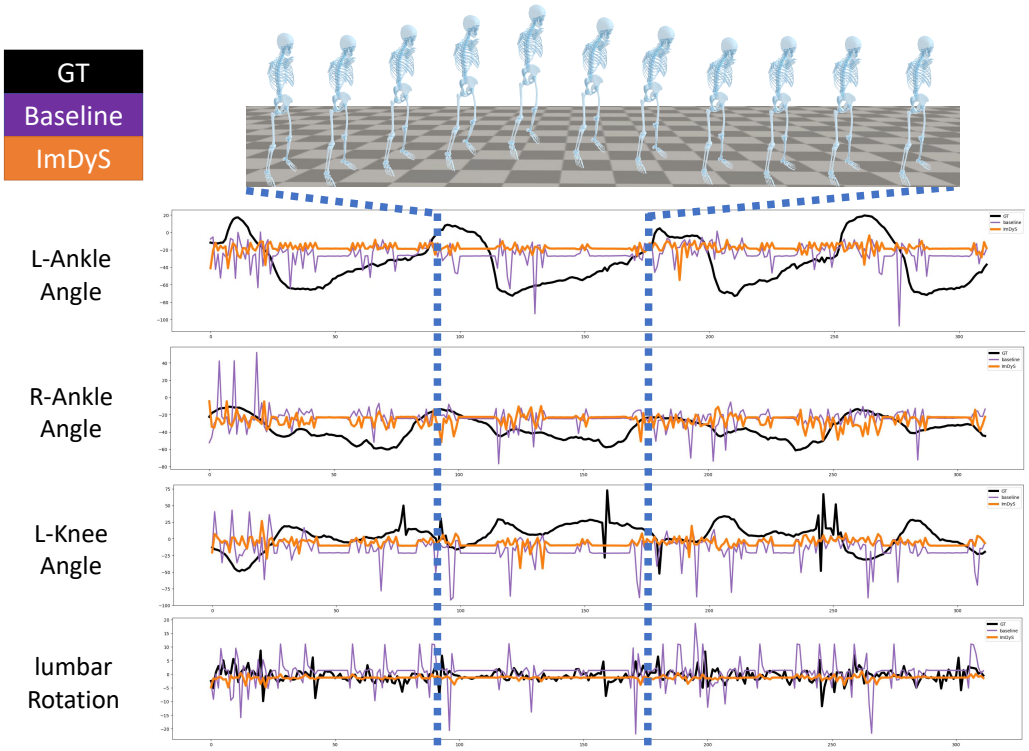

Figure 11: Visualization of a failed joint torque prediction case on AddBiomechanics. For the "jumping" motion, the baseline and ImDyS both perform sub-optimally. Neither of them correctly predicts the joint torques.

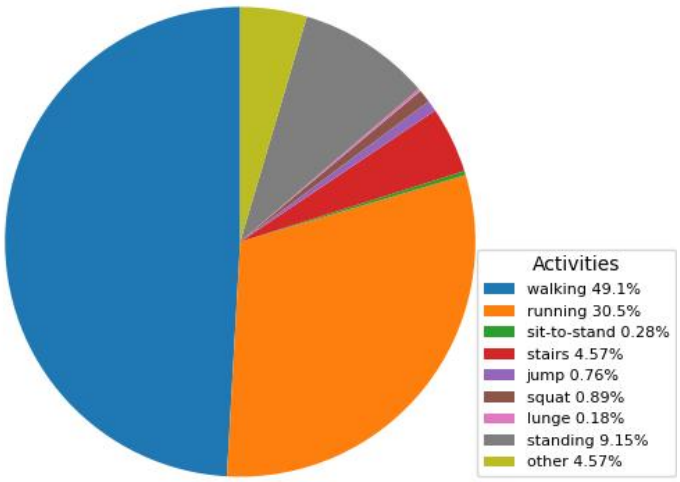

Figure 12: AddBiomechanics data distribution. Among all activities, walking and running account for over 75%, indicating that the amount of gait data is large

B AddBiomechanics Results Analysis

We visualize a failure case on the AddBiomechanics dataset in Fig. 11. As shown, neither the baseline nor ImDyS manages to faithfully predict the joint torques for the jumping motion. In the following, we discuss the reasons for the failure.

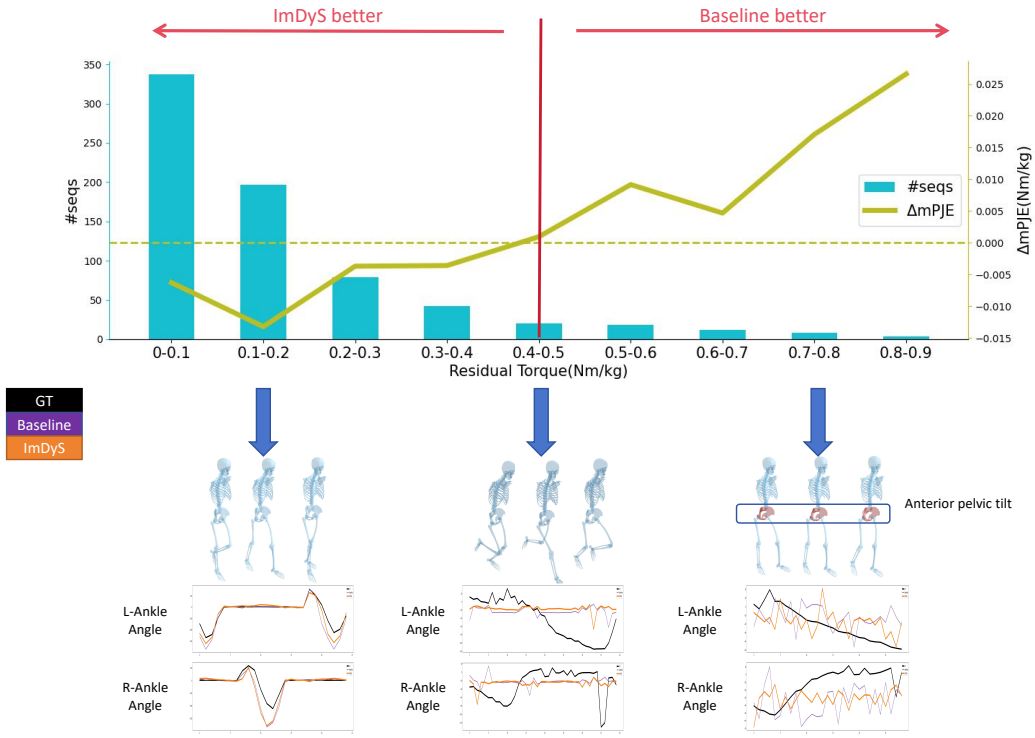

Figure 13: Relationship between data quality and model performance differences. Higher residual torque indicates lower data quality with lower reliability of the optimized GT torques. ΔmPJE is the difference between the mPJE of ImDyS and the baseline. #seqs is the number of sequences. With the residual torque increasing, the baseline provides lower mPJE than ImDyS, indicating the baseline overfits low-quality data. Instead, ImDyS, with the knowledge inherited from ImDy, shows less overfitting for these cases.

Data distribution. Fig. 12 shows the data distribution of AddBiomechanics (Werling et al., 2024). As shown, over 75% of the data are either walking, running, or standing, which are extremely limited. Though ImDyS is empowered with the diverse ImDy, it still requires data to learn the mapping between simulated torques and real torques for non-gait data. These result in ImDyS' poor performance when processing non-gait data. Further mitigating the limited data issue for non-gait motions would be a meaningful goal to pursue.

Data quality. Besides the distribution, the quality is also limited in AddBiomechanics. As shown in Fig. 11, joint torques for some joints (like the lumbar) suffer from unstable optimization with jittering results. According to Werling et al. (2024), 21.2% of AddBiomechnics are classified with clinical-grade high quality (residual torque $<$ 0.1 * body weight * height). There exists a 1.6829 Nm/kg average root residual torque of the optimized GTs in AddBiomechanics, which is considerably higher than the mPJE of ImDyS (0.1626 Nm/kg). We further analyze the relationship between the data quality and the model performances. We adopt residual torques as an indicator of the data quality and calculate ΔmPJE=mPJE$_{ImDyS}$-mPJE$_{Baseline}$ of sequences with different residual torques. Notice that higher residual torque indicates lower data quality with lower reliability of the optimized GT torques. Results are shown in Fig. 13. As shown, some samples could suffer from bad kinematics fitting (like the unnatural anterior pelvic tilt in Fig. 13), resulting in less reliable GT optimized joint torques. An interesting phenomenon is that the lower the residual torques are, the better ImDyS performs, which means ImDyS performs better for high-quality samples. This indicates the baseline might overfit low-quality data with high residual torques. Instead, ImDyS, with the knowledge inherited from the large-scale diverse ImDy, manages to resist the negative influences from low-quality samples. We also show how the mPJE of ImDyS changes with data quality in Fig. 14. As shown, the performance of ImDyS degenerates synchronously with data quality.

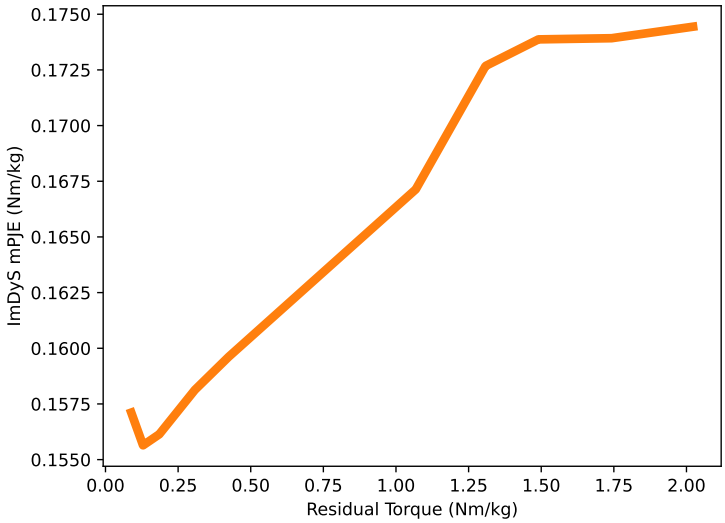

Figure 14: Relationship between data quality and ImDyS performance. Higher residual torque indicates lower data quality with lower reliability of the optimized GT torques. The performance of ImDyS degenerates synchronously with data quality.

Table 7: Per-Joint mPJE of ImDyS for samples with clinical-grade quality.

	Right mPJE$_\tau$ ↓		Left mPJE$_\tau$ ↓	
Joint Name	ImDyS	Baseline	ImDyS	Baseline
Hip Flexion	**0.267**	0.270	**0.273**	0.274
Hip Adduction	**0.196**	0.212	**0.198**	0.199
Hip Rotation	**0.087**	0.109	**0.083**	0.098
Knee	0.193	**0.188**	**0.195**	0.209
Ankle	0.197	**0.195**	0.202	**0.199**
Subtalar	**0.069**	0.071	**0.079**	0.084
MTP	**0.0005**	0.0006	**0.0007**	0.0008
Lumbar Extension	**0.328**	0.339	-	-
Lumbar Bending	**0.255**	**0.255**	-	-
Lumbar Rotation	**0.113**	**0.113**	-	-

Per-Joint Performance Analysis. It is also noticeable in Fig. 11 that the gap between GT and prediction differs for different joints. To this end, we further analyze the per-joint performance of ImDyS. The per-joint mPJE of ImDyS and the per-joint mPJE of ImDyS in each frame for samples with clinical-grade quality (residual torque $<$ 0.1 body weight * height) is demonstrated in Tab. 7. ImDyS manages to improve the performance on most joints compared to the baseline without ImDy, especially for the hips. An interesting phenomenon is that ImDyS performs slightly better on the right half of the body.